Opt Quant Electron (2017) 49:281
DOI 10.1007/s11082-017-1119-z

Computational analysis of solitons all-optical logic NAND and XNOR gates using semiconductor optical amplifiers

Amer Kotb[1,2]

Received: 9 April 2017 / Accepted: 26 July 2017 / Published online: 31 July 2017

Abstract Solitons all-optical logic NAND and XNOR gates using semiconductor optical amplifiers-assisted Mach–Zehnder interferometers are computationally analyzed at a data rate of 80 Gb/s. The investigation of the output quality factor is included. All-optical logic gates are capable of operating at 80 Gb/s with logical correctness and acceptable quality.

Keywords Soliton · NAND gate · XNOR gate · Semiconductor optical amplifier · Mach–Zehnder interferometer

1 Introduction

Because of dispersion, waves with different frequencies will travel at different velocities and their shape will, therefore, change over time. The shape of soliton wave pulses does not change during propagation because of a balance between the nonlinear and dispersion effects in the medium. Several solitons-based operations of the key building blocks have been demonstrated (Agrawal 2002; Kubota and Odagaki 2013; Xu et al. 2014; Louis et al. 2010; Spatial soliton all-optical logic gates 2006). The semiconductor optical amplifier (SOA) is the most promising element due to its attractive features of strong nonlinearity, a potential for integration, high stability, low power consumption, and compactness. The phase and gain recovery times of SOA are slow which limit the operation speed to be <100 Gb/s. The device used to carry out these simulations is the Mach–Zehnder interferometer (MZI) which has two similar SOAs arms. The MZI is developed by Ludwig Mach and Ludwig Zehnder around 1892, which demonstrates light interference phenomena by a division of a light beam (Pereira et al. 2009). The MZI device is fabricated with

✉ Amer Kotb
asm05@fayoum.edu.eg; kotb@phys.uconn.edu; amer_22003@yahoo.com

[1] Physics Department, Faculty of Science, Fayoum University, Fayoum 63514, Egypt

[2] The Guo China-US Photonics Laboratory, Changchun Institute of Optics, Fine Mechanics, and Physics, Changchun 130033, China

tilted waveguides to reduce the reflections at the facets and to couple the light into the semiconductor waveguides. The MZI is widely used due to its low energy requirement, high stability, high coupling efficiency, low-temperature sensitivity, and compactness.

All-optical INVERT operations are readily accomplished by using the gain saturation scheme in SOAs. The performances of all-optical logic NAND and XNOR gates with SOAs' nonlinear effects have been presented (Kim et al. 2005, 2006; Saharia and Sharma 2014; Kotb et al. 2010, 2011; Son et al. 2007; Ye et al. 2006; Li et al. 2007; Kotb and Maeda 2012; Kang et al. 2009; Dong et al. 2009; Sotoa et al. 2004; Dutta and Wang 2013; Kotb 2012). Also, the NAND and XNOR gates using quantum-dots SOAs have been investigated (Kotb and Zoiros 2014; Dimitriadou and Zoiros 2012a b; Kotb and Zoiros 2013; Kotb 2015; Dimitriadou and Zoiros 2013). Other main types of interferometers employed in executing all-optical logic gates using SOA have been studied (Houbavlis and Zoiros 2003; Nazerian et al. 2016; Chattopadhyay and Roy 2011; Houbavlis et al. 1999; Zoiros and Demertzis 2011; Zoiros et al. 2008; Siarkos and Zoiros 2009). The previous works based on SOA-based all-optical gates (Kim et al. 2005, 2006; Saharia and Sharma 2014; Kotb et al. 2010, 2011; Son et al. 2007; Ye et al. 2006; Li et al. 2007; Kotb and Maeda 2012; Kang et al. 2009; Dong et al. 2009; Sotoa et al. 2004; Dutta and Wang 2013; Kotb 2012) have not taken into account the soliton pulses. The main novel aspect of the conducted work is that the consideration of the hyperbolic secant pulses instead of the Gaussian pulses. The hyperbolic secant pulse has narrower linewidth and broader wings than a Gaussian pulse. The hyperbolic secant input pulse has almost zero dispersion which leads to an acceptable quality. The obtained quality factor (Q-factor) in this work is higher than in previous publications (Kim et al. 2006; Saharia and Sharma 2014; Kotb et al. 2010, 2011; Son et al. 2007; Ye et al. 2006; Kim et al. 2005; Li et al. 2007; Kotb and Maeda 2012; Kang et al. 2009; Dong et al. 2009; Sotoa et al. 2004; Dutta and Wang 2013; Kotb 2012) in which the soliton input pulses have not been considered. The achieved Q-values are 32.65 and 28.7 for NAND and XNOR gates, respectively. In this study, our previous publications (Kotb 2016a, b, 2017; Kotb and Alamer 2016; Kotb and Zoiros 2016) have been completed and generalized by investigating the performances of solitons all-optical logic NAND and XNOR gates by means of a numerical simulation. The operation data rate used in this simulation is 80 Gb/s. The computer program has been prepared and run in Wolfram Mathematica®. The simulated Q-factor versus the dispersion constant, input pulse energy, injection current, pulse width, SOA's carrier lifetime, thickness & length of SOA's active region, linewidth enhancement factor (α-factor), and saturation (continues wave) power has been detailed examined and assessed. The impact of amplified spontaneous emission (ASE) has also been included.

2 SOA-MZI model

The operation of SOA-assisted MZI can be theoretically studied by solving the SOA-MZI's rate equations. More specifically, the carrier heating (CH) results from a thermalization of carriers in the entire energy band following the pulse. This is a fast process occurring in the time scale of 0.1–0.7 ps. The injection pulse reduces the gain at the photon energy of this pulse, i.e. in the gain spectrum it burns a hole. The process is known as spectral hole burning (SHB). By taking into consideration the effects both of CH and SHB, the time-dependent gain for each SOA is given by Dutta and Wang (2013), Kotb (2012)

$$\frac{dh(t)}{dt} = \frac{h_0 - h(t)}{\tau_C} - (exp\,[h(t) + h_{CH}(t) + h_{SHB}(t)] - 1)\,\frac{P(t)}{E_{sat}} \quad (1)$$

$$\frac{dh_{CH}(t)}{dt} = -\frac{h_{CH}(t)}{\tau_{CH}} - \frac{\varepsilon_{CH}}{\tau_{CH}}\,(exp\,[h\,(t) + h_{CH}(t) + h_{SHB}(t)] - 1)\,P(t) \quad (2)$$

$$\frac{dh_{SHB}(t)}{dt} = -\frac{h_{SHB}(t)}{\tau_{SHB}} - \frac{\varepsilon_{SHB}}{\tau_{SHB}}\,(exp\,[h\,(t) + h_{CH}(t) + h_{SHB}(t)] - 1)\,P(t) - \frac{dh(t)}{dt} - \frac{dh_{CH}(t)}{dt} \quad (3)$$

where functions 'h' represent the SOA's gain integrated over its length for carrier depletion-recombination, CH, and SHB, respectively. τ_c is the SOA's carrier lifetime and $\exp[h_0] = G_0$ is the SOA's unsaturated power gain. $E_{sat} = P_{sat}\,\tau_c$ is the SOA's saturation energy and P_{sat} is the SOA's saturation power. P(t) is the data power inserted into the SOAs, which is linked to the light intensity (S(t)) through $P(t) = \kappa\,S(t)$, where κ denotes the conversion factor from photon density to power. τ_{CH} and τ_{SHB} are the temperature relaxation rate and the carrier-carrier scattering rate, respectively. ε_{CH} and ε_{SHB} are the nonlinear gain suppression factors due to CH and SHB, respectively.

The total gain *G(t)* through the SOA-MZIs is given

$$G(t) = exp\,[h(t) + h_{CH}(t) + h_{SHB}(t)] \quad (4)$$

The carrier density-induced phase change is given

$$\Phi\,(t) = -0.5\,[\alpha\,h\,(t) + \alpha_{CH}\,h_{CH}(t)] \quad (5)$$

where α is the traditional linewidth enhancement factor. α_{CH} and α_{SHB} are the linewidth enhancement alpha factors due to CH and SHB, respectively. The value of α_{SHB} is zero because the SHB produces an asymmetrical spectral hole centered at the signal wavelength. In this case, the Kramers–Kronig integral becomes antisymmetric at the operating frequency and the Kramers–Kronig integral remains very small (Kotb 2015).

In this simulation, the input data streams pulses are assumed to be a hyperbolic-secant "sech" shape whose input power is described by Agrawal (2002)

$$P_{A,B}(t) = \sum_{n=1}^{n=N} a_{nA,B}\,P_{soliton}\,Sech^2\left[\frac{1.763\,(t - nT)}{\tau_{FWHM}}\right] \quad (6)$$

where $a_{nA,B}$ represents the n-th pulse for signals A and B, which takes the digital value of "1" or "0". T is the single bit period, e.g. T = 1000/data rate. nT is the pseudo-random binary sequence (PRBS) length, where T is the single bit period and $n = 2^7 - 1$ is the PRBS length. τ_{FWHM} is the full width at half maximum or the pulse width. The PRBS streams are available entirely in optical form and can be provided by the means of the appropriate optoelectronic circuits, which have been devised for this purpose (Zoiros et al. 2011). $P_{soliton}$ is the soliton peak power which is defined as (Mollenauer and Gordon 2006)

$$P_{soliton} = \left(\frac{1.763}{2\pi}\right)^2 \frac{A_{eff}\,\lambda^3}{n_2 c}\,\frac{D}{\tau_{FWHM}^2} \quad (7)$$

where c and λ are the velocity and wavelength in a vacuum, respectively. D is the dispersion constant, n_2 is the fiber nonlinear coefficient, and A_{eff} is the fiber effective area. The dispersion constant is defined as $D = (d/d\lambda)\, v_g^{-1}$, where v_g is the group velocity. The experimental values of D for a single mode fiber is ~0.3–1 ps/(nm.km), while the fixed values of the other two soliton-related parameters are $n_2 \sim 2.6 \times 10^{-16}$ cm^2/W and $A_{eff} \sim 5 \times 10^{-9}$ cm^2 (Mollenauer and Gordon 2006). The soliton propagation length at which the pulses return to their initial "sech" shape is given by Kubota and Odagaki (2013)

$$Z_{soliton} = 0.322 \frac{\pi^2 c \tau_{FWHM}^2}{D\lambda^2} \tag{8}$$

At the soliton pulses fixed FWHM of 2 ps and dispersion constant (D) range of 0.3–1 (ps/(nm km)), $Z_{soliton}$ is calculated to vary between 1.58 and 5.28 km for single mode optical fibers. The input soliton power is a few mW for $Z_{soliton}$ of hundreds of km.

3 NAND gate

3.1 Principle operation

In this work, the NAND gate is realized by a series combination of AND and INVERT gates as shown in Fig. 1. First SOA-MZI serves as an optical logic AND gate where data stream A (centered at λ_1) is coupled to port 1 while a low power continuous wave (CW) at wavelength λ_1 is launched into port 2. Concurrently, the probe data stream B at λ_2 is split at port 3 and sent into both SOAs. When data B = 0, no light centered at λ_2 is injected into the configuration to enable operation, which results in no output from port 4. When B = 1 and A = 0, the gain and phase shifts experienced by the split components of data stream B are the same in both SOAs which interfere destructively at port 4 giving a '0' as a logical outcome. When B = A = 1, the two replicas of data stream B will experience different gain and subsequently phase shift in the respective SOAs. Thus, on their recombination, they will interfere constructively at port 4 giving a '1' as a logical outcome. In this case, if the phase difference induced between them is made equal to π, maximum switching will

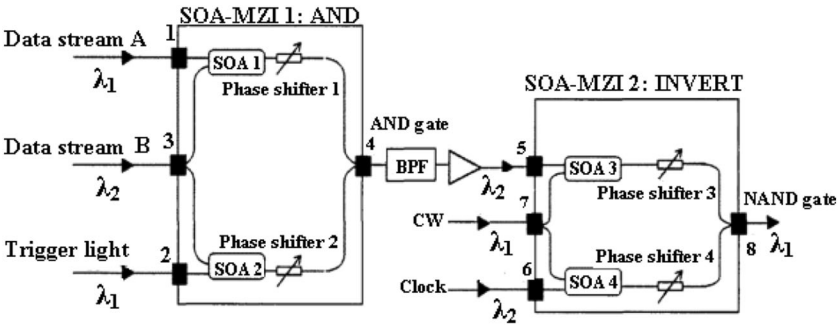

Fig. 1 Schematic diagram of a NAND gate using two series MZIs. BPF: band-pass filter

occur at the output. Only when both data A and B are '1', the MZI yield '1' at port 4, which is logic operation A AND B.

The A AND B output data stream is amplified to the proper power level by an amplifier and guided into port 5 as a data signal to one arm of the second MZI configured for INVERT operation. A clock pulse train with the same pulse shape and energy (centered at λ_2) is injected into port 6 as the probe while a CW light is injected into port 7 as a control beam. In this way, the result centered at λ_1 coming out from port 8 will be that of the modulo-2 addition of the data patterns of signals injection into ports 6 and 5, or INVERT (A AND B), which is the same as logic A NAND B.

3.2 Simulation

The input powers inside SOA1 for AND operation are defined as

$$P_1(t) = P_A(t) + P_B(t) \tag{9}$$

$$P_2(t) = 0.5\,P_B(t) + P_{delayed\,A}(t) \tag{10}$$

and inside SOA2 for NAND operation are

$$P_3(t) = P_{AND}(t) + 0.5\,P_{CW} \tag{11}$$

$$P_4(t) = 0.5\,P_{CW} + P_C(t) \tag{12}$$

The NAND output power after passing the MZIs is described by the following equation.

$$P_{NAND}(t) = 0.25\,P_{CW}\{G_1(t) + G_2(t) - 2\sqrt{G_1(t)\,G_2(t)}\,Cos[\Phi_1(t) - \Phi_2(t)]\} \tag{13}$$

in which Pc corresponds to the input power of the CW probe signal. $G_{1,2}(t)$ is the time-dependent gain and $\phi_{1,2}(t)$ is the phase shift in the arms of MZI. The values of the critical parameters used to simulate the NAND gate have been cited in Table 1.

The average power is roughly 4 mW. The input power is 40 times smaller than used in optical fibers to obtain the logic gates. The optical fiber is weak nonlinearities and requires

Table 1 Calculation parameters for NAND gate

Symbol	Definition	Value
E_0	Pulse energy	0.1 pJ
τ_{FWHM}	Pulse width	1.54 ps
τ_c	SOA's carrier lifetime	5 ps
P_{sat}	Saturation power	10 mW
α	Linewidth enhancement factor	3
α_{CH}	Linewidth enhancement factor due to CH	1
α_{SHB}	Linewidth enhancement factor due to SHB process	0
τ_{CH}	Temperature relaxation rate	0.3 ps
τ_{SHB}	Carrier-carrier scattering rate	0.1 ps
ε_{CH}	Nonlinear gain suppression factor due to CH	0.02 W^{-1}
ε_{SHB}	Nonlinear gain suppression factor due to SHB	0.02 W^{-1}
G_0	SOA's unsaturated power gain	30 dB

a high input intensity and long length to carry out the logic gates. During the operation, the average launched power of signals A & B is around 10 and 0.75 dBm for the clock light. The input powers are low consumption.

The Q-factor gives the information for the optical signal to noise ratio, and is defined as $Q = (S_1 - S_0)/(\sigma_1 + \sigma_2)$ (Dutta and Wang 2013; Kotb 2012), where S_1, S_0 are the average intensities of the expected '1's, '0's and σ_1, σ_2 are the standard deviations of these intensities. The Q-factor relates to the bit-error rate and directly proportional to the difference of powers between bit 1 and bit 0. For an ideal amplifier with the soliton input pulses, the obtained output Q-value is 32.65 at 80 Gb/s. Figure 2 shows the simulation's results and the corresponding eye diagram for the soliton NAND operation.

The dispersion is the spreading out of the pulses. The pulses are overlapping and the transmitted data will be lost due to the dispersion. The dispersion power saturates the SOAs more easily, which results in a fall of Q-value. The Q-factor decreases with increasing the dispersion constant as shown in Fig. 3 at $G_0 = 10$ and 30 dB.

The simulated Q-factor depends on the pulse energy and injection current at different D values for NAND operation as shown in Fig. 4. The calculation is carried out by setting the SOA's active region thickness of 0.2 μm, the effective length of 2 mm, and FWHM or pulse width of all input data streams of 1.5 ps. As shown in Fig. 4a, an increasing in the input pulse energy saturates the SOAs easily, which decreases the Q-value. From this figure, it can be seen that, even for the highest considered dispersion value, the Q-factor attains its required minimum of six for an input pulse energy which is equivalent to an average power of roughly 4 mW. The increasing in injection current causes an increasing of free carrier densities which increases the recombination processes. The Q-factor increases with increasing the injection current as shown in Fig. 4b. For high Q-factor, the amplifier should be operated at current larger than the starter current (turn-on current).

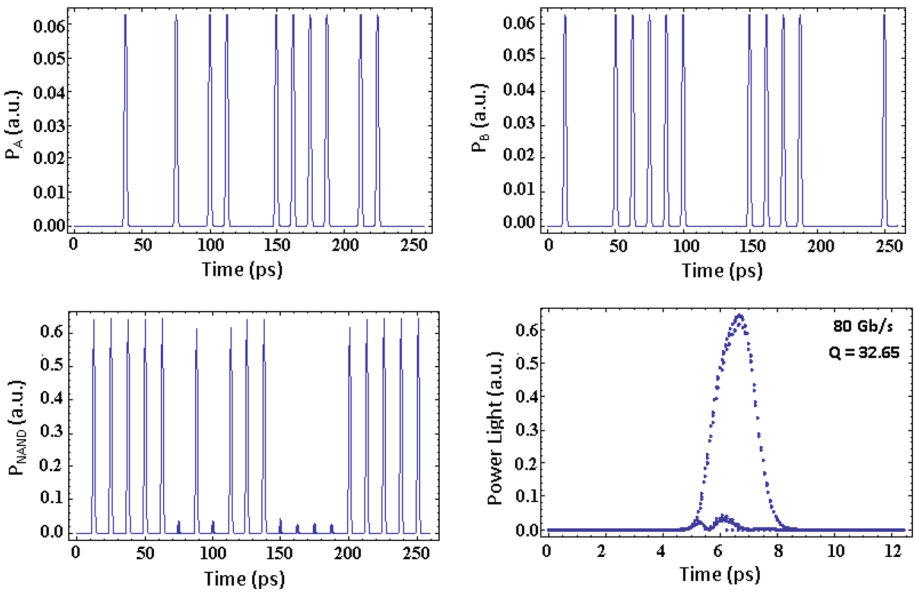

Fig. 2 Simulation results and eye diagram for NAND operation

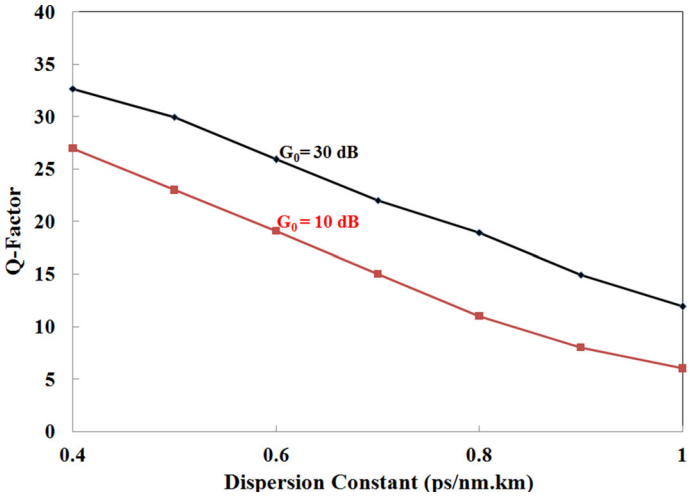

Fig. 3 Simulated Q-factor versus dispersion constant for NAND operation

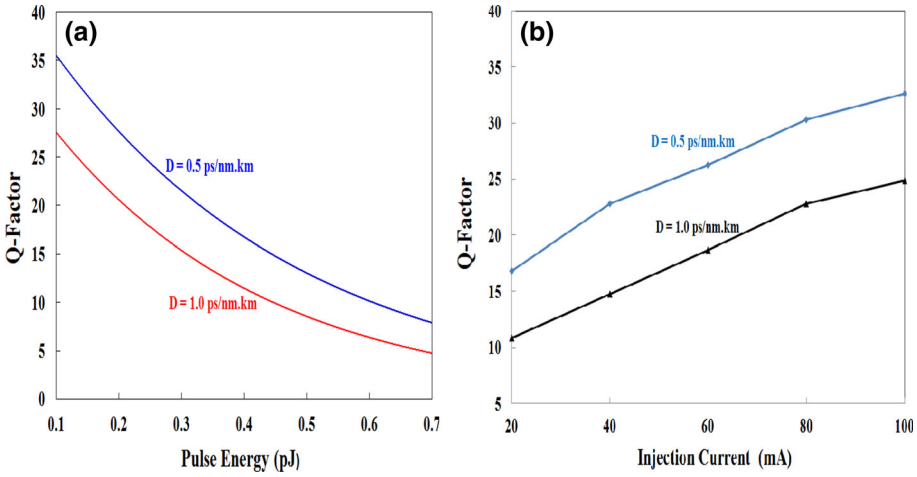

Fig. 4 Q-factor versus **a** pulse energy and **b** injection current for NAND operation

The Q-factor as a function of pulse width and SOA's carrier recombination lifetime is shown in Fig. 5. As shown in Fig. 5a, the Q-factor decreases with increasing the pulse width because two neighboring pulses are spreading out and emerging which leads to the pulses distortion. The eye pattern is poor quality with large amplitude noise and small opening. To decrease the dispersion, the pulse width should be small and the gaps between pulses should be large. For fast operations, the carrier lifetime should be small (Kotb et al. 2011; Kotb 2012). The SOA's carrier lifetime is achieved owing to the CW signal which is launched into the MZI during the simulations of NAND and NXOR gates. The SOA's carrier lifetime determines the speed of gain and phase recovery in the active region so Q-factor is higher for a shorter carrier lifetime as shown in Fig. 5b. Generally, long lifetime causes carriers depletion of SOA which leads to pulse distortion, this would limit the pulse repetition rate in high-speed transmission.

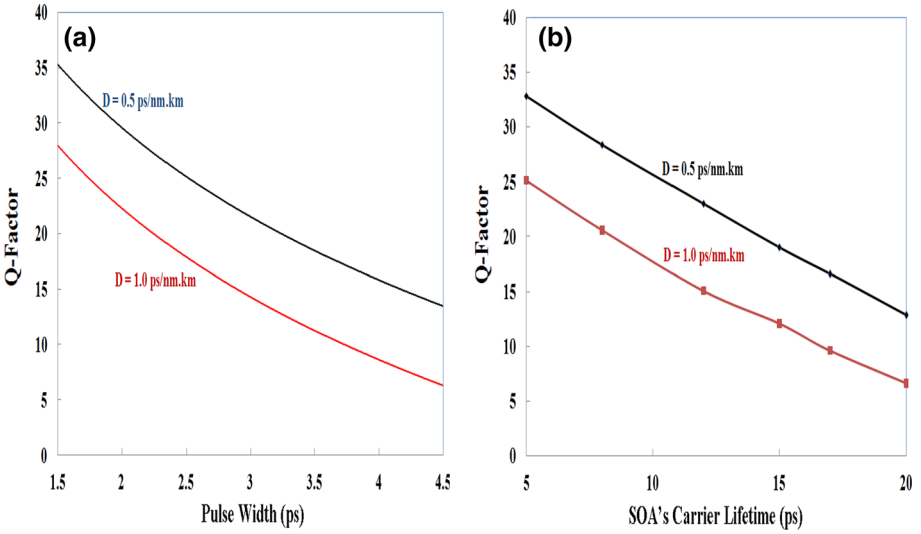

Fig. 5 Simulated Q-factor versus **a** pulse width and **b** SOA's carrier lifetime for NAND operation

The calculated Q-factor depends on length and thickness of the SOA's active region as shown in Fig. 6. The typical SOA's length is between 0.6 and 2 mm. With increasing the SOA's length the overall gain increases exponentially and then the Q-factor as shown in Fig. 6a. Simulated Fig. 6a has been simulated at two different injection currents. The thickness of the SOA's active region is typically in the range of 0.1–0.5 μm. The thick active region is used for fast gain recovery and hence fast performance of SOA. The optical gain region is determined by the thickness. The carrier densities increase with increasing the active region thickness and hence the Q-factor as shown in Fig. 6b.

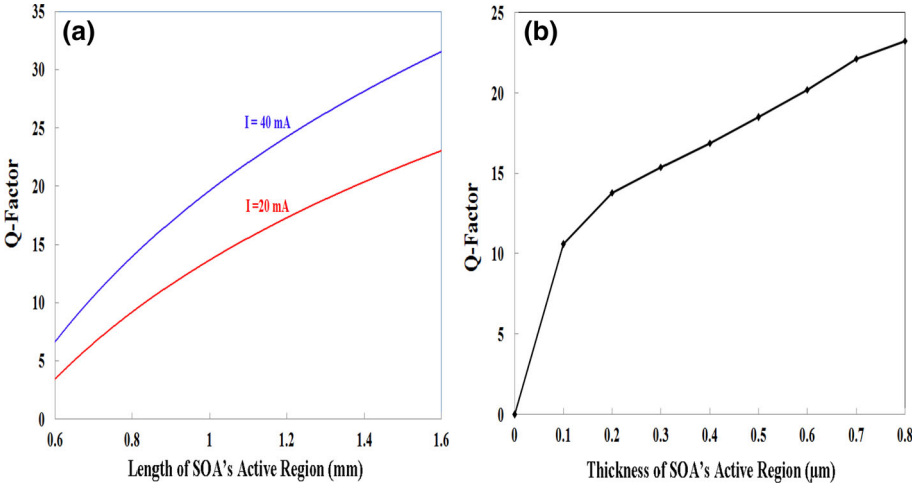

Fig. 6 The simulated Q-factor depends on **a** length and **b** thickness of the SOA's active region for NAND operation

The semiconductor materials used in SOA should be direct band gaps and lattices matching for the radiative recombination processes. Much of the recent experimental works have been carried out by using InGaAsP/InP. The InGaAsP material has an optical gain concerned around 1300 or 1550 nm. The linewidth enhancement factor (α-factor) depends on the relative position of the amplifier gain peak and the signals' wavelengths. The α-factor reflects the link between phase and gain changes as clear in Eq. (5). The phase changes are increasing at large α-factor. The increasing in α-factor is directly caused by the increase of free carrier density and hence, the Q-value as shown in Fig. 7 at two different D values.

When the pump pulse isn't injection into the SOA, the gain of the continues wave (CW) power becomes very high and hence its output power. Increasing of the input CW power or the saturation power (P_{sat}) reduces the carrier recovery time and then increases the output Q-factor as shown in Fig. 8. The CW power is approximately equal to 0.01 P_{sat}.

At zero injection current, the spontaneous emissions appear and amplify that it causes high noise through the amplifier. The amplified spontaneous emission (ASE) measures the position of the gain peak, the pulse width (FWHM) of the gain curve and the gain ripple. The large ASE increases the average intensity power of "0" which decreases the Q-value. The ASE power is related to the spontaneous emission factor (N_{SP}) and added numerically to the input data streams to obtain the Q-factor using the following equation (Kotb 2012):

$$P_{ASE} = N_{SP}(G_0 - 1)\, h\upsilon B_0 \tag{14}$$

where h is Planck's constant, G_0 is an unsaturated gain, B_0 is an optical bandwidth, and at optical frequency υ. This simulation has been carried out at $G_0 = 30$ dB, $B_0 = 3$ nm, and $\lambda = 1550$ nm which has low loss propagation.

The Q-factor versus N_{sp} is shown in Fig. 9 at two different D values and unsaturated gains (G_0) of 10 and 30 dB. The effect of ASE can be experimentally verified by adding a wideband (few nm wide) optical unmodulated signal to the streams data with negligible saturation effects. Modeling and experiments of the ASE in SOAs are detailed investigated

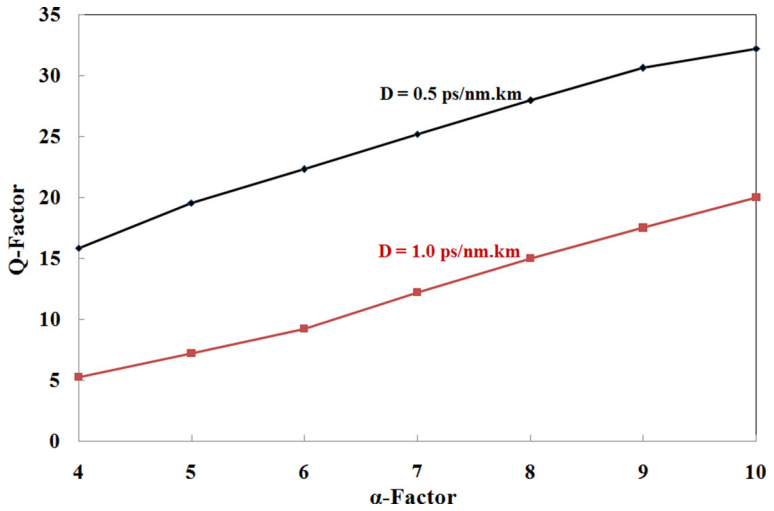

Fig. 7 Dependence of the simulated Q-factor on linewidth enhancement factor (α-factor) at two different D values for NAND operation

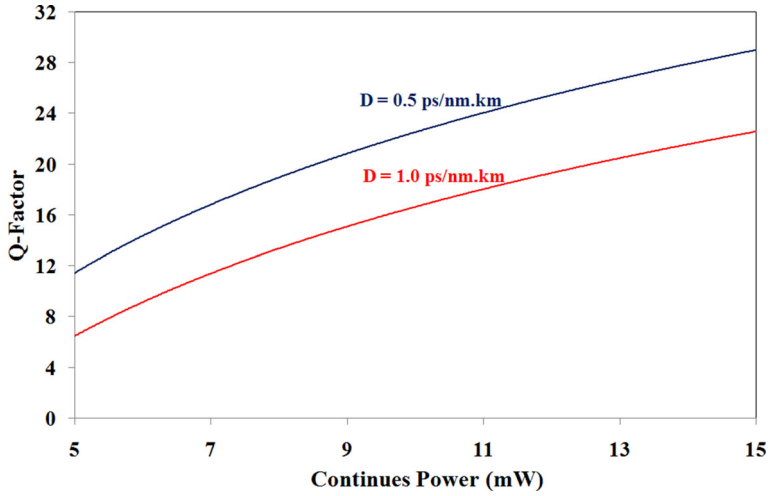

Fig. 8 Calculated Q-factor versus continues wave power at two different D values for NAND operation

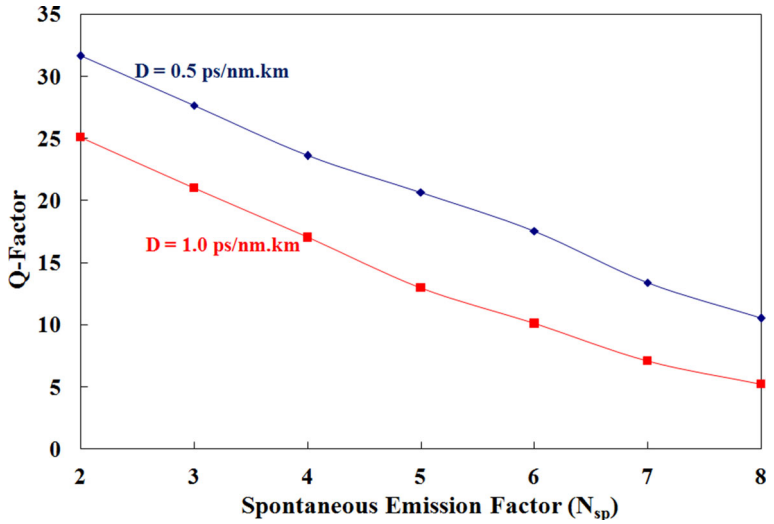

Fig. 9 Calculated Q-factor versus spontaneous emission factor (N_{sp}) at two different D values for NAND operation

in Ref. (Talli and Adams 2003). The study of ASE effects is useful for cascaded logic operations.

4 XNOR gate

4.1 Principle operation

In this study, the XNOR gate is realized by a series combination of XOR and INVERT gates as shown in Fig. 10. For XOR operation, two data signals A and B are injected into

the SOAs incorporated in the upper and lower arms of first MZI. A clock stream comprising of continuous '1's is introduced in the setup from the middle input port of the configuration. The data signal A at λ_1 and B at λ_3 induce a phase shift in the split components of the clock signal at λ_2 in each SOA. Then, the recombined clock signal at the output of first MZI carries the result of the XOR operation between the binary content of data signals A and B. Initially, MZI1 is balanced, and so when A = 0 and B = 0, the decomposed clock signal components traveling through the two MZIs do not acquire any phase shift in the respective SOAs. Thus, when they recombine at the output the result is 0. However, when A = 1 and B = 0, the clock signal replica traveling through the upper arm together with signal A acquires a phase change, while its counterpart traveling through the lower arm does not suffer any such change. This results in '1' at the output. The same happens when A = 0, B = 1. However, when A = 1 and B = 1, the phase changes induced on the clock signal constituents traveling through both MZI arms are equal, hence the output is 0. The INVERT operation is obtained similarly to the XOR operation if one of the data inputs is replaced by a clock signal. Then in order to realize the XNOR operation, the XOR output from MZI1 is launched into the upper arm of second MZI. Concurrently, a continuous wave (CW) beam and another clock signal are launched into the middle and bottom input ports, respectively. The effect of ASE on the performance of the XNOR gate is due to the contribution both from the XOR and INVERT operations.

4.2 Simulation

The simulation has been carried out by run Wolfram Mathematica to solve the rate equations of the SOA. The critical parameters used to carry out this simulation have been cited in Table 2.

The input powers for XOR operation is given by:

$$P_1(t) = P_A(t) + 0.5\,P_{CW} \tag{15}$$

$$P_2(t) = 0.5\,P_{CW} + P_B(t) \tag{16}$$

and for XNOR operation is given by:

$$P_3(t) = P_{XOR}(t) + 0.5\,P_{CW} \tag{17}$$

$$P_4(t) = 0.5\,P_{CW} + P_C(t) \tag{18}$$

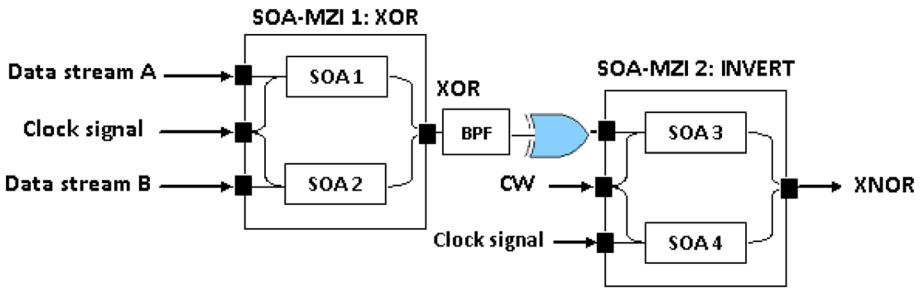

Fig. 10 Schematic diagram of XNOR gate using two series MZIs. BPF: band-pass filter

Table 2 Calculation parameters for XNOR gate

Symbol	Definition	Value
E_0	Pulse energy	0.17 pJ
τ_{FWHM}	Pulse width	1.5 ps
τ_c	SOA's carrier lifetime	5 ps
P_{sat}	Saturation power	10 mW
α	Linewidth enhancement factor	2
α_{CH}	Linewidth enhancement factor due to CH	1
α_{SHB}	Linewidth enhancement factor due to SHB process	0
τ_{CH}	Temperature relaxation rate	0.3 ps
τ_{SHB}	Carrier-carrier scattering rate	0.1 ps
ε_{CH}	Nonlinear gain suppression factor due to CH	0.02 W^{-1}
ε_{SHB}	Nonlinear gain suppression factor due to SHB	0.02 W^{-1}
G_0	SOA's unsaturated power gain	30 dB

Figure 11 shows the simulation results and the corresponding eye diagram of the soliton XNOR operation. The achieved Q-value is 28.7 at 80 Gb/s.

For XNOR output, the simulated Q-factor versus dispersion constant is shown in Fig. 12 for G_0 of 10 and 30 dB. All-optical continuously tunable delay line system based on wavelength conversion in SOAs and group-velocity dispersion in a dispersion-compensating fiber is investigated (Hu et al. 2008).

The output Q-factor as a function of pulse energy and injection current at different D values for XNOR operation is shown in Fig. 13.

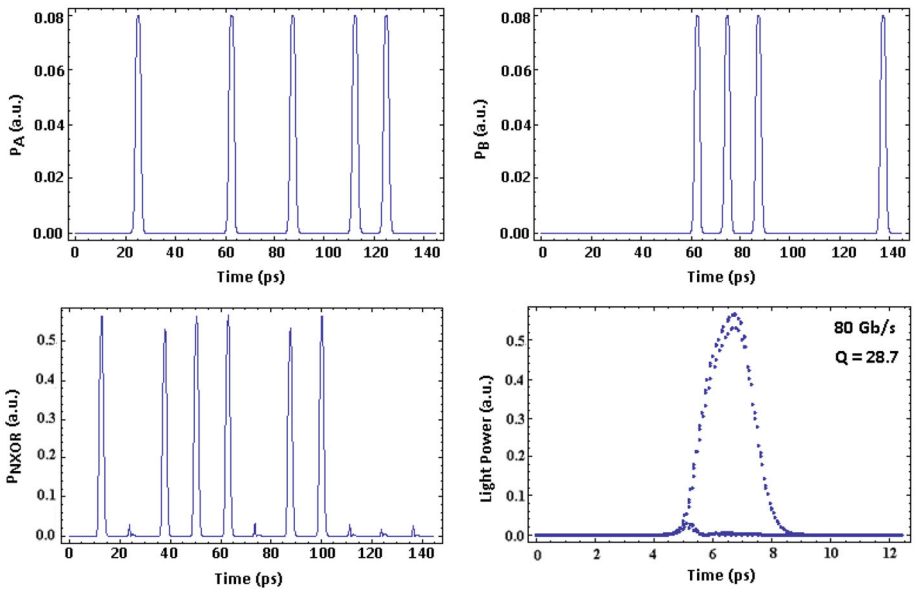

Fig. 11 Simulation results and the corresponding eye diagram for XNOR operation

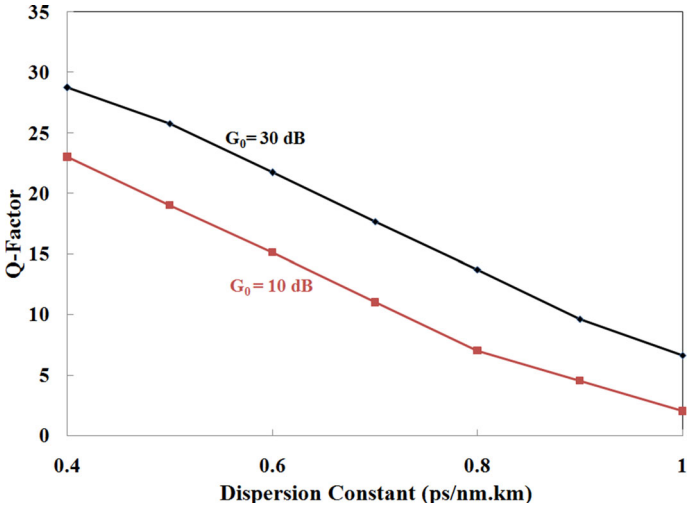

Fig. 12 Simulated *Q*-factor versus dispersion constant for XNOR operation

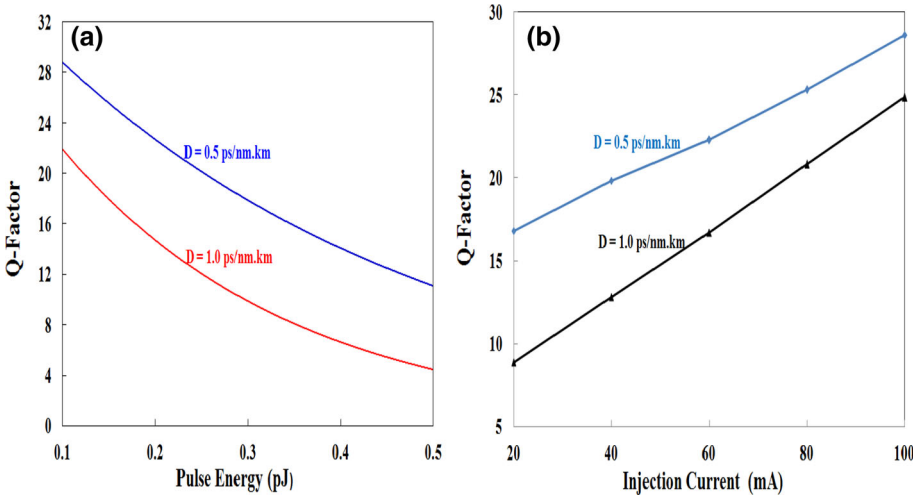

Fig. 13 Q-factor versus pulse energy and injection current at different D values for XNOR operation

The dependence of Q-factor on pulse width and SOA lifetime is shown in Fig. 14.

The increasing in α-factor causes an increasing in the Q-value as shown in Fig. 15. This simulation is carried out at two different D values.

The ASE noise adds a noise term to the output bits ''0'' and ''1''. Thus a larger ASE noise would increase the average intensity of the ''0'' level and hence reduce the output Q-factor. The pattern effect output noises of ''1'' and ''0'' determine the standard deviation (σ_1, σ_2) used in the Q-factor calculation. The simulated Q-factor versus N_{sp} is shown in Fig. 16 at two different D values.

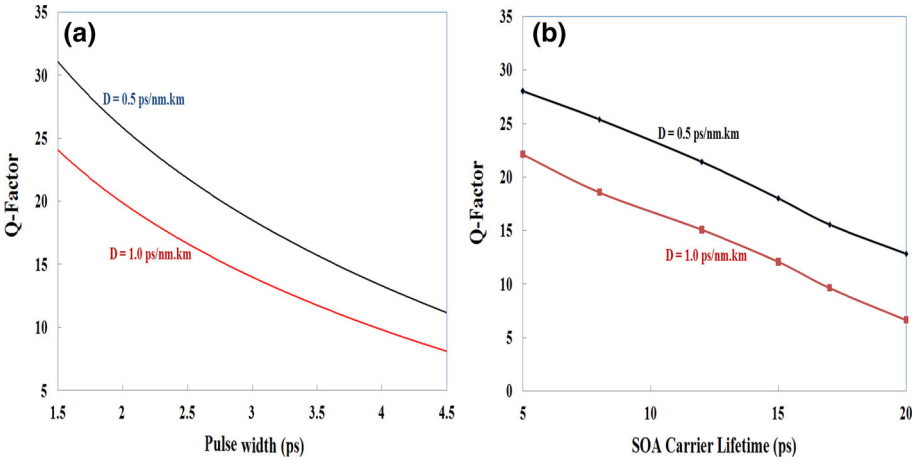

Fig. 14 Dependence of Q-factor on **a** pulse width and **b** SOA lifetime for XNOR operation

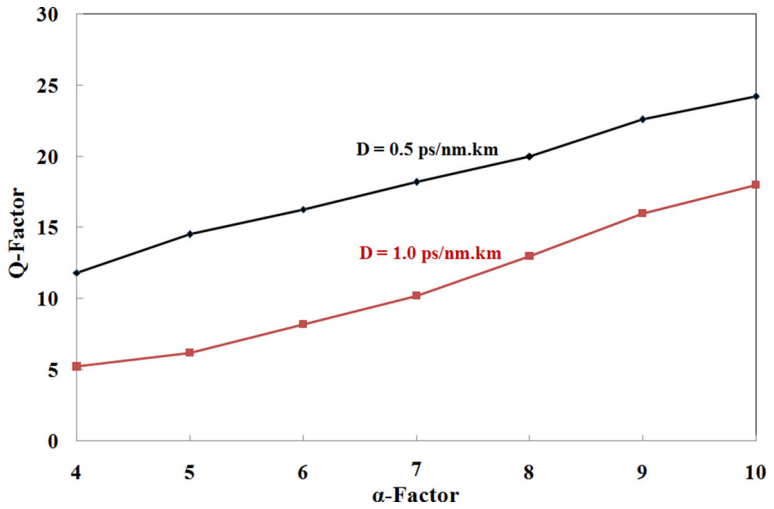

Fig. 15 Q-value as a function of α-factor for XNOR operation

The experimental and theoretical studies on an actively mode-locked fiber ring laser (FRL)-based on a single SOA to generate an external optical pulse train is presented (Zoiros et al. 2000). The source is easily constructed from commercially available components and produces 4.3 ps pulses at 10 and 20 GHz over a tuning range of 16 nm. This configuration results in a stable oscillator since the use of a single active element to provide both gain and modulation renders the cavity short. Furthermore, the cavity is nearly polarization insensitive as there is no lithium niobate modulator and the SOA is operated under heavy saturation providing nearly polarization-independent gain. One consequence of using a cavity with a single active, optically modulated SOA is its ability to produce mode-locked pulses at a harmonic repetition frequency of the external signal.

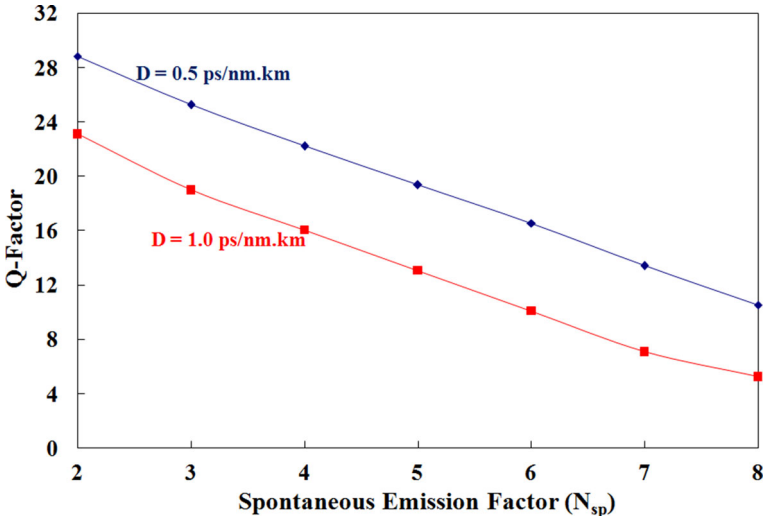

Fig. 16 Simulated Q-factor versus Nsp for XNOR operation

A mathematical model of the FLR is describing the mode-locking process in the laser oscillator and providing solutions for the steady-state mode-locked pulse profile. The model enables the prediction of the duration of the mode-locked pulse that exits the FLR source versus the duration of the external pulse that is inserted into the system. A complete investigation of the critical parameters that determine the width, energy, and position of the mode-locked pulse relative to the external pulse has been performed (Zoiros et al. 2000). These parameters are including the small signal gain and carrier lifetime of the SOA, the cavity loss, the pulse energy and width of the external modulating signal. It has been found both experimentally and theoretically that the minimum pulse width is obtained when these parameters are adjusted so that the mode-locked pulse forms midway between two successive external pulses and that this condition corresponds to the case where the energies of the external and mode locked pulses are nearly equal. A rule of thumb is also given concerning the relationship between the operating repetition period and the SOA's carrier lifetime which is particularly important when the FRL source is used for ultrafast all-optical applications.

5 Conclusion

In this simulation, solitons all-optical logic NAND and XNOR gates with semiconductor optical amplifiers (SOAs)-assisted a Mach–Zehnder interferometer are simulated and investigated at a data rate of 80 Gb/s. For a dispersion constant of 0.5 ps/nm km, the achieved output quality factor (Q-factor) is 32.65 for NAND and 28.7 for XNOR which is well above the limit for error-free performance. The calculated Q-factor decreases with increasing the pulse width and the spontaneous emission factor. The Q-factor increases with increasing the injection current, the linewidth enhancement factor (α-factor), and the saturation power or continues wave power. The extracted results show that the treated logic gate is capable of operating at 80 Gb/s with logical correctness and with the defined metric

being more than adequate. The input soliton pulses have a hyperbolic-secant amplitude that can be experimentally carried out by using a mode-locked laser source.

References

Agrawal, G.P.: Applications of Nonlinear Fiber Optics. Academic Press, USA (2002)

Chattopadhyay, T., Roy, J.N.: Semiconductor optical amplifier (SOA)-assisted Sagnac switch for designing of all-optical tri-state logic gates. Optik **122**, 1073–1078 (2011)

Dimitriadou, E., Zoiros, K.E.: On the design of reconfigurable ultrafast all-optical NOR and NAND gates using a single quantum-dot semiconductor optical amplifier-based Mach–Zehnder interferometer. Opt. **14**(105401), 1–9 (2012a)

Dimitriadou, E., Zoiros, K.E.: On the feasibility of ultrafast all-optical NAND gate using single quantum-dot semiconductor optical amplifier-based Mach–Zehnder interferometer. Opt. Laser Technol. **44**, 1971–1981 (2012b)

Dimitriadou, E., Zoiros, K.E.: Proposal for ultrafast all-optical XNOR gate using single quantum-dot semiconductor optical amplifier-based Mach–Zehnder interferometer. Opt. Laser Technol. **45**, 79–88 (2013)

Dong, J., Zhang, X., Huang, D.: A proposal for two-input arbitrary Boolean logic gates using single semiconductor optical amplifier by picosecond pulse injection. Opt. Express **17**, 7725–7730 (2009)

Dutta, N.K., Wang, Q.: Semiconductor Optical Amplifiers, 2nd edn. World Scientific Publishing Company, Singapore (2013)

Houbavlis, T., Zoiros, K.E.: SOA-assisted Sagnac switch and investigation of its roadmap from 10 to 40 GHz. Opt. Quantum Electron. **35**, 1175–1203 (2003)

Houbavlis, T., Vlachos, K., Zoiros, K., Papakyriakopoulos, T., Avramopoulos, H., Girardin, F., Guekos, G., Dall'Ara, R., Hansmann, S., Burkhard, H.: All-optical XOR in a semiconductor optical amplifier-assisted fiber Sagnac gate. IEEE Photon. Technol. Lett. **11**, 334–336 (1999)

Hu, Z., Sun, J., Liu, L., Wang, J.: All-optical tunable delay line based on wavelength conversion in semiconductor optical amplifiers and dispersion in dispersion-compensating fiber. Appl. Phys. B **91**, 421–424 (2008)

Kang, I., Rasras, M., Buhl, L., Dinu, M., Cabot, S., Cappuzzo, M., Gomez, L.T., Chen, Y.F., Patel, S.S., Dutta, N., Piccirilli, A., Jaques, J., Giles, C.R.: All-optical XOR and XNOR operations at 86.4 Gb/s using a pair of semiconductor optical amplifier Mach–Zehnder interferometers. Opt. Express **12**, 19062–19066 (2009)

Kim, S.H., Kim, J.H., Choi, J., Woo, D.H.: All-optical NAND gate using cross-gain modulation in semiconductor optical amplifiers. Electron. Lett. **2**, 957–959 (2005)

Kim, J.Y., Kang, J.M., Kim, T.Y., Han, S.K.: All-optical multiple logic gates with XOR, NOR, OR, and NAND functions using parallel SOA-MZI structures: theory and experiment. Lightwave Technol. **24**, 3392–3399 (2006)

Kotb, A.: All-Optical Logic Gates Using Semiconductor Optical Amplifiers. Lambert Academic Publishing, Saarbrucken (2012)

Kotb, A.: Modeling of high-quality factor XNOR gate using quantum-dot semiconductor optical amplifiers at 1 Tb/s. Braz. J. Phys. **45**, 288–295 (2015)

Kotb, A.: Simulation of soliton all-optical logic XOR gate with semiconductor optical amplifier. Opt. Quantum Electron. **48**(307), 1–11 (2016a)

Kotb, A.: Numerically simulation of soliton OR gate with semiconductor optical amplifier-assisted delayed interferometer. Opt. Quantum Electron. **48**(462), 1–12 (2016b)

Kotb, A.: Theoretical analysis of soliton NOR gate with semiconductor optical amplifier-assisted Mach–Zehnder interferometer. Opt. Quantum Electron. **49**(180), 1–12 (2017)

Kotb, A., Alamer, F.A.: Dispersion on all-optical logic XOR gate using semiconductor optical amplifier. Opt. Quantum Electron. **48**(327), 1–10 (2016)

Kotb, A., Maeda, J.: All-optical logic NXOR based on semiconductor optical amplifiers with the effect of amplified spontaneous emission. Optoelectron. Lett. **8**, 437–440 (2012)

Kotb, A., Zoiros, K.E.: Simulation of all-optical logic XNOR gate based on quantum-dot semiconductor optical amplifiers with amplified spontaneous emission. Opt. Quantum Electron. **45**, 1213–1222 (2013)

Kotb, A., Zoiros, K.E.: 1 Tb/s high-quality factor NAND gate using quantum-dot semiconductor optical amplifiers in Mach–Zehnder interferometer. Comput. Electron. **13**, 555–561 (2014)

Kotb, A., Zoiros, K.E.: Soliton all-optical logic AND gate with semiconductor optical amplifier-assisted Mach–Zehnder interferometer. Opt. Eng. **55**(087109), 1–7 (2016)

Kotb, A., Ma, S., Chen, Z., Dutta, N.K., Said, G.: All-optical logic NAND based on two-photon absorption in semiconductor optical amplifiers. Opt. Commun. **283**, 4707–4712 (2010)

Kotb, A., Ma, S., Chen, Z., Dutta, N.K., Said, G.: Effect of amplified spontaneous emission on semiconductor optical amplifier based all-optical logic. Opt. Commun. **284**, 5798–5803 (2011)

Kubota, Y., Odagaki, T.: Logic Gates Based on Soliton Transmission in the Toda Lattice. Adv. Appl. Phys. **1**, 29–38 (2013)

Li, P., Huang, D., Zhang, X., Zhu, G.: Single-SOA-based all-optical XNOR and AND gates. In: Proceedings of SPIE 6782 (2007)

Louis, K., Perumal, S., Gopi, D.: Soliton-based logic gates using spin ladder. Commun. Nonlinear Sci. Numer. Simul. **15**, 3900–3912 (2010)

Mollenauer, L.F., Gordon, J.P.: Solitons in Optical Fibers: Fundamentals and Applications. Elsevier Academic Press, USA (2006)

Nazerian, V., Nasrabadi, A.T., Afrakoti, I.E.: Switching characteristics of SOA-assisted all-optical Sagnac interferometer switch for picoseconds pulse. Eng. Appl. Sci. **11**, 751–759 (2016)

Pereira, A., Ostermann, F., Cavalcanti, C.: On the use of a virtual Mach–Zehnder interferometer in the teaching of quantum mechanics. Phys. Educ. **44**, 281–291 (2009)

Saharia, A., Sharma, R.: An approach for Realization of all-optical NAND gate using nonlinear effect in SOA. Int. J. Signal Proc. Imaging Eng. **1**, 13–17 (2014)

Serak, S.V., Tabiryan, N.V., Peccianti, M., Assanto, G.: Spatial soliton all-optical logic gates. IEEE Photon. Technol. Lett. **18**, 1287–1289 (2006)

Siarkos, T., Zoiros, K.E.: Performance of single semiconductor optical amplifier-based ultrafast nonlinear interferometer with clock-control signals timing deviation in dual rail-switching mode. Opt. Eng. **48**, 85004–85012 (2009)

Son, C.W., Kim, S.H., Jhon, Y.M., Byun, Y.T., Lee, S., Woo, D.H., Kim, S.K., Yoon, T.H.: Realization of all-optical XOR, NOR, and NAND gates in a single format by using semiconductor optical amplifiers. Jpn. J. Appl. Phys. **46**, 232–234 (2007)

Sotoa, H., Alvareza, E., Dıaz, C.A., Topomondzo, J., Erasmeb, D., Schares, L., Occhi, L., Guekos, G., Castro, M.: Design of an all-optical NOT XOR gate based on cross-polarization modulation in a semiconductor optical amplifier. Opt. Commun. **237**, 121–131 (2004)

Talli, G., Adams, M.J.: Amplified spontaneous emission in semiconductor optical amplifiers: modeling and experiments. Opt. Commun. **218**, 161–166 (2003)

Xu, M., Li, Y., Zhang, T., Luo, J., Ji, J., Yang, S.: The analysis of all-optical logic gates based with tunable femtosecond soliton self-frequency shift. Opt. Express **22**, 8349–8366 (2014)

Ye, X., Ye, P., Zhang, M.: All-optical NAND gate using integrated SOA-based Mach–Zehnder interferometer. Opt. Fiber Technol. **12**, 312–316 (2006)

Zoiros, K.E., Demertzis, C.: On the data rate extension of semiconductor optical amplifier-based ultrafast nonlinear interferometer in dual rail switching mode using a cascaded optical delay interferometer. Opt. Laser Technol. **43**, 1190–1197 (2011)

Zoiros, K., Stathopoulos, T., Vlachos, K., Hatziefremidis, A., Houbavlis, T., Papakyriakopoulos, T., Avramopoulos, H.: Experimental and theoretical studies of a high repetition rate fiber laser, mode-locked by external optical modulation. Opt. Commun. **180**, 301–315 (2000)

Zoiros, K.E., Avramidis, P., Koukourlis, C.S.: Performance investigation of semiconductor optical amplifier-based ultrafast nonlinear interferometer in nontrivial switching mode. Opt. Eng. **47**(11), 115006–115011 (2008)

Zoiros, K.E., Das, M.K., Gayen, D.K., Maity, H.K., Chattopadhyay, T., Roy, J.N.: All-optical pseudorandom binary sequence generator with TOAD-based D flip-flops. Opt. Commun. **284**, 4297–4306 (2011)